Earth Surface Processes and Landforms
Earth Surf. Process. Landforms **29**, 687–711 (2004)
Published online in Wiley InterScience (www.interscience.wiley.com). DOI: 10.1002/esp.1064

LANDSLIDE INVENTORIES AND THEIR STATISTICAL PROPERTIES

BRUCE D. MALAMUD,[1]* DONALD L. TURCOTTE,[2] FAUSTO GUZZETTI[3] AND PAOLA REICHENBACH[3]

[1] *Department of Geography, King's College London, Strand, London, WC2R 2LS, UK*
[2] *Department of Geology, University of California, Davis, CA 95616 USA*
[3] *CNR–IRPI Perugia, via della Madonna Alta 126, Perugia, 06128, Italy*

Received 11 March 2003; Revised 22 August 2003; Accepted 31 October 2003

ABSTRACT

Landslides are generally associated with a trigger, such as an earthquake, a rapid snowmelt or a large storm. The landslide event can include a single landslide or many thousands. The frequency–area (or volume) distribution of a landslide event quantifies the number of landslides that occur at different sizes. We examine three well-documented landslide events, from Italy, Guatemala and the USA, each with a different triggering mechanism, and find that the landslide areas for all three are well approximated by the same three-parameter inverse-gamma distribution. For small landslide areas this distribution has an exponential 'roll-over' and for medium and large landslide areas decays as a power-law with exponent −2·40. One implication of this landslide distribution is that the mean area of landslides in the distribution is independent of the size of the event. We also introduce a landslide-event magnitude scale $m_L = \log(N_{LT})$, with N_{LT} the total number of landslides associated with a trigger. If a landslide-event inventory is incomplete (i.e. smaller landslides are not included), the partial inventory can be compared with our landslide probability distribution, and the corresponding landslide-event magnitude inferred. This technique can be applied to inventories of historical landslides, inferring the total number of landslides that occurred over geologic time, and how many of these have been erased by erosion, vegetation, and human activity. We have also considered three rockfall-dominated inventories, and find that the frequency–size distributions differ substantially from those associated with other landslide types. We suggest that our proposed frequency–size distribution for landslides (excluding rockfalls) will be useful in quantifying the severity of landslide events and the contribution of landslides to erosion.

KEY WORDS: landslides; earthquakes; erosion; natural hazards; frequency-size statistics; intensity scale

INTRODUCTION

Landslides are a complex natural phenomenon that constitutes a serious natural hazard in many countries (Brabb and Harrod, 1989). Landslides also play a major role in the evolution of landforms. The term 'landslide' includes a wide variety of slope movements, such as soil slips, deep-seated slides, mud flows, debris flows, rockfalls, etc. (Varnes, 1978; Pierson and Costa, 1987; Hutchinson, 1988; Cruden and Varnes, 1996; Hungr *et al*., 2001). Landslides are commonly associated with a trigger, such as an earthquake, a rapid snowmelt, or an intense rainfall, with landslide areas spanning more than eight orders of magnitude and landslide volumes more than twelve orders. Slope failures – ranging from single to tens of thousands – generally occur within minutes after an earthquake trigger, hours to days after a snowmelt trigger, and days to weeks after an intense rainfall trigger.

In order to quantify the occurrence of landslides it is necessary to have applicable data. In this paper, we will concentrate on the frequency–size statistics of landslides from landslide inventories. Landslide inventories usually give total landslide areas, with areas including both the failure and runout. It can be argued that just the landslide failure area or the landslide volume would be preferable, but these quantities are often difficult to determine. Rockfall-dominated inventories will be examined separately, as we consider the applicable physics to be fundamentally different.

Landslide inventories generally fall into two classes: (1) landslide-event inventories that are associated with a trigger; and (2) historical (geomorphological) landslide inventories, which are the sum of one or many landslide events over time in a region. An inventory of 'fresh' landslides can be substantially complete if detailed

* Correspondence to: B. D. Malamud, Environmental Monitoring and Modelling Research Group, Department of Geography, King's College London, Strand, London, WC2R, 2LS, UK. E-mail: bruce@malamud.com

mapping has been carried out shortly after the landslide event. Historical landslide inventories include events that have occurred over periods of tens, hundreds or even thousands of years. A characteristic of historical landslide inventories is that evidence of the existence of many of the smaller landslides has been lost due to various degrees of modification by subsequent landslides, erosional processes, anthropic influences, and vegetation growth. All evidence of smaller landslides is likely to be lost, and the borders of landslides become harder to distinguish with the passage of time.

There is accumulating evidence that in many historical and fresh-event landslide inventories, the frequency–area distribution of medium and large landslides decays as an inverse power of the landslide area (Fujii, 1969; Whitehouse and Griffiths, 1983; Ohmori and Hirano, 1988; Sasaki *et al*., 1991; Noever, 1993; Sugai *et al*., 1994; Yokoi *et al*., 1995; Pelletier *et al*., 1997; Hovius *et al*., 1997, 2000; Dai and Lee, 2001; Guzzetti *et al*., 2002; Dussauge-Peisser *et al*., 2002; Dussauge *et al*., 2003). This common behaviour is despite large differences in landslide types, sizes, distributions, patterns, and triggering mechanisms.

In this paper we fit a three-parameter inverse-gamma distribution to the frequency–area statistics of 'fresh' landslides for three landslide events, each the result of a different type of trigger. This distribution decays as an inverse power of the landslide area for medium and large landslides, and has an exponential rollover for small landslides. The inventories are substantially complete and well-documented, and consist of: (1) more than 11 000 landslides triggered by the 17 January 1994 Northridge (California) earthquake (Harp and Jibson, 1995, 1996); (2) more than 4000 landslides triggered by a snowmelt event in the Umbria region of Italy following a sudden temperature change on 1 January 1997 (Cardinali *et al*., 2000); (3) more than 9000 landslides triggered by heavy rainfall in Guatemala during late October and early November 1998 from Hurricane Mitch (Bucknam *et al*., 2001).

These three landslide-event inventories are in excellent agreement with our proposed probability distribution, which we hypothesize has general applicability. One implication is that the average area of landslides that occur in a landslide event will be the same for every 'complete' inventory. Another implication is the ability to define a 'magnitude' for each landslide event. This can be done by specifying the total number, total area, and/or the total volume of landslides in a landslide event. If a landslide inventory is incomplete (i.e. smaller landslides are not included), the partial inventory can be compared with our landslide probability distribution, and the corresponding landslide-event magnitude inferred. The principal purpose of this paper is to explore the validity and implications of the hypothesis that our proposed probability distribution has general applicability.

LANDSLIDE INVENTORY MAPS

The statistics of landslides – including their area, shape, location, etc. – are influenced by the accuracy of techniques used in compiling, mapping and digitizing the statistics. Because of their importance in compiling landslide frequency–size statistics, we will now consider a number of issues related to landslide inventory maps, including their preparation and limitations.

Inventory maps

It is recognized that landslide inventories are the simplest form of landslide mapping (Hansen, 1984; Wieczorek, 1984; Guzzetti *et al*., 1999). An inventory map records the location and, when known, the date of occurrence and types of landslides that have left discernible traces in an area. The different techniques used to prepare inventory maps depend on (1) the reason the map is being prepared, (2) the extent of the study area, (3) the scales of base maps and aerial photographs, and (4) the resources available to carry out the work (Guzzetti *et al*., 1999). Landslide maps can be prepared by collecting historical information on individual landslide events, or from the analysis of aerial photographs coupled with field surveys. The former is a means of constructing a landslide archive (IGS-WPWLI, 1990) and reports the location of sites where landslides are known to have occurred (Reichenbach *et al*., 1998). The latter are geomorphological maps that portray the distribution of landslide deposits (Rib and Liang, 1978; Guzzetti *et al*., 1999).

Geomorphological inventory maps may show (1) a *landslide-event inventory*, consisting of all the slope failures associated with a single trigger, such as an earthquake, rainstorm or snowmelt, or (2) a *historical landslide inventory*, the sum of many landslide events over a period of tens, hundreds or even many thousands of years. By interpreting multiple sets of aerial photographs of different ages, 'multi-temporal inventory' maps can be prepared. Usually,

a single map is used to portray all different types of landslides. Alternatively, a set of maps can be prepared, each map showing a different type of failure, i.e. deep-seated slides, shallow failures, debris flows, rockfalls, etc.

Landslide inventories can be compiled at different scales from a variety of sources. Small-scale inventories (<1:200 000) can be compiled through inquires to public organizations and private consultants, by searching chronicles, journals, technical and scientific reports (Radbruch-Hall *et al*., 1982) or by interviewing landslide experts ('archive' inventories, e.g. Reichenbach *et al*., 1998). Small-scale landslide maps can also be obtained through aerial photograph analysis (Cardinali *et al*., 1990). Medium-scale landslide inventories (1:25 000 to 1:200 000) are prepared through the systematic interpretation of aerial photographs at print scales 1:60 000 to 1:20 000 and by integrating local field checks with historical information. Large-scale inventories (>1:25 000, e.g. Guzzetti *et al*., 2003a) are prepared, usually for limited areas, using both the interpretation of aerial photographs at print scales >1:20 000 and extensive field investigations that use a variety of techniques and tools pertaining to geomorphology, engineering geology and geotechnical engineering (Wieczorek, 1984).

Recognition of landslide features from stereoscopic aerial photographs is a complex, largely empirical technique that requires experience, training, a systematic methodology and well-defined interpretation criteria (Speight, 1977; Rib and Liang, 1978). As they are prepared by interpreting one or more sets of aerial photographs and correcting the results by field mapping, geomorphological inventory maps tend to be subjective. Many factors affect the reliability, completeness and resolution of an inventory map, including: (1) landslide freshness and age; (2) the quality and scale of aerial photographs and base maps; (3) the morphological and geological complexity of the study area; (4) land use types and alterations; and (5) the degree of experience of the geomorphologist involved.

Limitations of inventory maps

Once a landslide is recognized in the field or from aerial photographs it must be mapped, i.e. information about the landslide's location and characteristics is obtained and transferred onto paper. This operation is not trivial and is error-prone. Since absolute coordinates of the boundaries of a landslide are seldom available, the geomorphologist uses available base maps and the topographical and morphological features shown on the map to locate the landslide. Where the topographic map is accurate and shows the actual morphology, and where landslides have a distinct morphological signature, locating and mapping the landslide is straightforward and subject to little uncertainty. Where the topographic map does not represent faithfully the morphology or the landslide is not very distinct, location and mapping errors are possible.

In placing the landslide on the topographic map, the geomorphologist uses all of the information on the map, including the position and shape of divides and drainage lines, the pattern of vegetation and land use, and the presence of anthropic objects (e.g. roads, buildings, etc.). If these are not shown correctly or are incomplete, the mapping can be affected by errors and uncertainties. Consequently, the reliability of a landslide inventory map varies spatially, depending on morphology, hydrography, land-use pattern, presence of forest, and abundance and location of anthropic elements. In addition, for large-scale landslide inventory maps (>1:20 000) the landslide and the topographic information are strictly coupled, thus landslides should be shown only with the topographic maps used to prepare the inventory. Once the landslide has been mapped on paper, the information is digitized for further analysis and display. This second step in the production of a landslide inventory is also error-prone, and can introduce a variety of cartographic errors, some severe. An error in the location of a landslide boundary of only 1–2 mm on the topographic map (i.e. 10–20 m on the ground at 1:10 000 scale) may result in >5 per cent difference in landslide area for small (<1 ha) slope failures.

After landslides are transferred to a GIS (geographical information system), computations of landslide areas are possible. Any vector-based GIS system can calculate the area and perimeter of polygons used to represent the landslide. Thus, for a single landslide, computation of its area is straightforward. If the landslide deposit is mapped separately from the crown or depletion zone, the two will have to be combined before the total landslide area is computed. This operation can be performed automatically in a GIS, provided the polygons representing the landslides were properly coded. The coding operation is usually simple, but time-consuming, particularly for large datasets. Landslide areas and perimeters obtained from the GIS are planar (i.e. projected) measurements that differ from the real ones. Ideally, one would prefer to know the actual area and perimeter of a landslide. Where a digital elevation model is available, local slope can be computed in a GIS and measurements of

landslide perimeter and area corrected for topographic gradient. However, this is seldom done, and frequency–area statistics of landslides are normally from projected values.

In many landscapes, landslides tend to occur where they have occurred in the past. Thus, in many parts of the world, landslides occur in clusters. A cluster may contain several landslides of different sizes, types, and ages. Computing the area of these clusters of landslides is relatively easy, and can be achieved by removing all internal boundaries between different landslide elements (polygons). This is a simple operation in a GIS if polygons were properly coded. Removing internal boundaries gives the total area affected by landslides, but will not provide the correct statistics for individual landslide areas or the number of landslides. Knowing the extent of each slope failure in a landslide cluster is difficult, and requires some inference. This is certainly a problem for the analysis of the frequency–size statistics of landslides, and cannot be corrected rapidly or automatically. It requires extensive manual work in a GIS, and some interpretation to infer the boundary of older landslides below the newer ones. This effect is important for historical inventories, where landslides of many generations and sizes can overlap. The use of a historical inventory map improperly corrected for overlapping landslide polygons will result in an underestimation of the largest landslides.

Clusters of adjacent and overlapping landslides can also form as a result of an individual trigger, over a period of minutes to a few days. Coalescence of multiple small slope failures into a larger landslide area may locally prevent the correct identification of the smallest failures. Landslide coalescence introduces a bias towards the smallest failures and is particularly important where soils slips, debris flows, debris avalanches, rockfalls, and other shallow disrupted failures affect incoherent soils (e.g. loose volcanic rocks).

Completeness of landslide inventories

Landslide inventory maps record the location of all landslides that have left discernible features in an area. These features may not be recognized in the field or through the interpretation of aerial photographs, as they are often obscured by erosion, vegetation, urbanization, and anthropic action including ploughing. Thus, landslide inventories are generally incomplete and the level of completeness of the inventory is unknown, particularly for historical inventories. Indeed, estimating the completeness of a landslide inventory is a difficult task.

Immediately after a landslide event, individual landslides are ‘fresh’ and usually clearly recognizable. The boundaries between the failure areas (depletion, transport and depositional areas) and the unaffected terrain are usually distinct, making it relatively easy for the geomorphologist to identify and map the landslide. This is particularly true for small, shallow landslides, such as soil slips or debris flows (apart from the problem of landslide coalescence, as discussed above).

For large, complex slope movements, the boundary between the stable terrain and the failed mass is transitional, particularly at the toe. The limit may also be transitional along the sides, where tension cracks arranged in an *en échelon* pattern are common. For large deep-seated landslides, identifying the exact limit of the failed mass may not be easy even for fresh failures, particularly in urban or forest areas. Areas affected by even the largest and most catastrophic landslide events are seldom investigated exhaustively, because investigators concentrate in the areas where landslides were more abundant or where the damage was most severe or widespread.

Landslide boundaries become increasingly indistinct with the age of the landslide. This is caused by various factors, including local adjustments of the landslide to the new morphological setting, new landslides, and erosion. Historical landslide inventories are the sum total of single to many landslide events that occurred over time in a region. They become more and more incomplete with time due to two linked factors. First, the evidence for small landslides is removed by erosion, growth of vegetation, and human activities. Second, landslide boundaries become increasingly indistinct, making the landslides themselves much harder to identify on aerial photographs.

A formal definition of completeness requires that a landslide inventory includes *all landslides* associated with a landslide event (a single trigger) or multiple landslide events over time (historical). This definition assumes that all landslides are visible and recognizable, and that the entire study area affected, even marginally, by the trigger(s) is fully and thoroughly investigated. For practical reasons, these criteria are never met.

A functional definition of completeness requires that the landslide inventory includes a substantial fraction of all landslides at all scales. The tools and techniques available to compile the inventory must be able to meet this requirement within the study area. An important attribute of this definition is that a substantially complete inventory *must* include a substantial fraction of the smallest landslides. This definition may be applicable to

landslide-event inventories, but not to historical inventories, because many smaller- and intermediate-size landslides in historical inventories have been erased by erosion and anthropic action.

LANDSLIDE FREQUENCY–AREA DISTRIBUTIONS

We now use three substantially complete landslide inventories to obtain the dependence of landslide frequency on landslide area. Other inventories, dominated by falls, will be considered separately in a rockfall section. Variables used in this paper are given in Table I.

We first define a pdf (probability density function) $p(A_L)$ according to

$$p(A_L) = \frac{1}{N_{LT}} \frac{\delta N_L}{\delta A_L} \tag{1}$$

Table I. Variables used in text

Variable	Description	Equation introduced
$\delta N_L/\delta A_L$	δN_L is the number of landslides with areas between A_L and $A_L + \delta A_L$.	1
ε	Coefficient in $V_L = \varepsilon A_L^{1.50}$.	19
$\Gamma(\xi)$	Gamma function, $\Gamma(\xi) = \int_0^\infty y^{\xi-1} \exp(-y)\,dy$, $\xi > 0$.	3
$\Gamma(\xi, \eta)$	Incomplete gamma function, $\Gamma(\xi, \eta) = \int_\eta^\infty y^{\xi-1} \exp(-y)\,dy$, $\xi > 0$.	7
ρ	Parameter primarily controlling power-law decay for medium and large values in three-parameter inverse-gamma probability distribution.	3
a	Parameter primarily controlling location of maximum probability in three-parameter inverse-gamma probability distribution.	3
A_L	Area of landslide.	1
$\bar{A}_L$	Average area of landslides in an inventory.	11
$A_{LC}(\geq A_L)$	The cumulative area of all landslides in an inventory with areas greater than or equal to A_L.	16
$A_{L\max}$	Maximum landslide area in an inventory.	23
A_{LT}	Total area of landslides in an inventory	15
$f(A_L)$	Frequency density of landslide areas: the number of landslides δN_L with areas between A_L and $A_L + \delta A_L$, divided by the width of that bin, δA_L.	35
$f(V_L)$	Frequency density of landslide volumes: the number of landslides δN_L with volumes between V_L and $V_L + \delta V_L$, divided by the width of that bin, δV_L.	39
$f(V_R)$	Frequency density of rockfall volumes: the number of rockfalls δN_R with volumes between V_R and $V_R + \delta V_R$, divided by the width of that bin, δV_R.	38
M	Earthquake magnitude.	36
m_L	Magnitude of a landslide event, with $m_L = \log N_{LT}$.	31
$N_{LC}(\geq A_L)$	Cumulative number of landslides with areas greater than or equal to A_L.	24
N_{LT}	Total number of landslides in an inventory.	1
$p(A_L)$	Probability density: the frequency density, $f(A_L)$, divided by the total number of landslides in a substantially complete landslide inventory, N_{LT}.	1
s	Parameter primarily controlling exponential rollover for small values in three-parameter inverse-gamma probability distribution.	3
V_L	Volume of landslide.	18
$\bar{V}_L$	Average volume of landslides in an inventory.	20
$V_{L\max}$	Maximum landslide volume in an inventory.	27
V_{LT}	Total volume of landslides in an inventory.	20
V_R	Volume of rockfall.	38

Table II. Properties and predictions for three landslide distributions

Attribute	Source of Number*	Northridge earthquake†	Umbria snowmelt‡	Guatemala rainfall§
Study area (km^2)		10 000	2000	10 000
Total number of landslides, N_{LT}	Inventory	11 111	4233	9594
Mean area of landslides, $\bar{A}_L$ (km^2)	Inventory	$2{\cdot}14 \times 10^{-3}$	$3{\cdot}01 \times 10^{-3}$	$3{\cdot}07 \times 10^{-3}$
	1	$3{\cdot}07 \times 10^{-3}$	$3{\cdot}07 \times 10^{-3}$	$3{\cdot}07 \times 10^{-3}$
Total area of landslides, A_{LT} (km^2)	Inventory	23·8	12·7	29·5
	2	34·1	13·0	30·6
Largest landslide area, $A_{L\max}$ (km^2)	Inventory	0·259	0·156	3·87
	3	0·851	0·425	0·762
Mean volume of landslides, $\bar{V}_L$ (km^3)	**4**	$1{\cdot}08 \times 10^{-5}$	$1{\cdot}65 \times 10^{-5}$	$5{\cdot}59 \times 10^{-5}$
	5	$0{\cdot}89 \times 10^{-5}$	$1{\cdot}36 \times 10^{-5}$	$2{\cdot}87 \times 10^{-5}$
	6	$2{\cdot}28 \times 10^{-5}$	$2{\cdot}03 \times 10^{-5}$	$2{\cdot}24 \times 10^{-5}$
Total volume of landslides, V_{LT} (km^3)	**4**	$1{\cdot}20 \times 10^{-1}$	$6{\cdot}79 \times 10^{-2}$	$5{\cdot}36 \times 10^{-1}$
	5	$0{\cdot}99 \times 10^{-1}$	$5{\cdot}75 \times 10^{-2}$	$2{\cdot}76 \times 10^{-1}$
	7	$2{\cdot}53 \times 10^{-1}$	$8{\cdot}57 \times 10^{-2}$	$2{\cdot}15 \times 10^{-1}$
Landslide-event magnitude m_L	**8**	4·04	3·63	3·98
	9	3·89	3·61	3·98

* Key: **1**, Theoretical mean area of landslides $\bar{A}_L$ from Equation 14 with $a = 1{\cdot}28 \times 10^{-3}$ km^2, $s = -1{\cdot}32 \times 10^{-4}$ km^2, and $\rho = 1{\cdot}40$.
2, Total area of landslides A_{LT} based on theoretical $\bar{A}_L$ and inventory N_{LT} using Equation 15.
3, Theoretical $A_{L\max}$ obtained from inventory N_{LT} using Equation 26.
4, Each landslide volume V_L is obtained from inventory A_L using Equation 19.
5, Each landslide volume V_L is obtained from inventory A_L using Equation 18.
6, Mean volume of landslides $\bar{V}_L$ obtained from inventory N_{LT} using Equation 30.
7, Total volume of landslides V_{LT} obtained from inventory N_{LT} using Equation 33.
8, Landslide-event magnitude m_L obtained from inventory N_{LT} using Equation 31.
9, Landslide-event magnitude m_L obtained from inventory A_{LT} using Equation 32.
† Landslides triggered by earthquake, 17 January 1994, Northridge, California, USA (Harp and Jibson, 1995, 1996).
‡ Landslides triggered by rapid snowmelt, January 1997, Umbria, Italy (Cardinali *et al*., 2000; Guzzetti *et al*., 2002).
§ Landslides triggered by heavy rainfall from Hurricane Mitch, late October/early November 1998, Guatemala (Bucknam *et al*., 2001).

where δN_L is the number of landslides with areas between A_L and $A_L + \delta A_L$, and N_{LT} is the total number of landslides in the inventory. We increase our bin width δA_L with increasing area A_L, so that bin widths are approximately equal in logarithmic coordinates. The pdf defined in Equation 1 satisfies the normalization condition

$$\int_0^\infty p(A_L)dA_L = 1 \tag{2}$$

This normalization requires a substantially complete landslide inventory. We will first derive an applicable pdf using three substantially complete landslide-event inventories (see Table II for inventory details), and then later discuss how this pdf can be applied to partially complete inventories.

Our first example is an inventory of landslides triggered by the magnitude 6·7 Northridge (California, USA) earthquake, on 17 January 1994. The inventory, covering about 10 000 km^2, was obtained by Harp and Jibson (1995, 1996) through extensive field mapping that started immediately after the earthquake, and their systematic analysis of high-altitude aerial photography, taken at a nominal scale of 1:60 000 within hours of the earthquake. The inventory contains 11 111 landslides, for a total landslide area of 23·8 km^2 (0·24 per cent of the study area), with an average density over the study area of about 1·1 landslides per square kilometre. However, most landslides were concentrated in just 10 per cent of the study area that includes the Santa Susana Mountains and the mountains north of the Santa Clara River valley. Harp and Jibson (1995) found that most of the slope failures were shallow (1–5 m) disrupted falls and slides in weakly cemented Tertiary to Pleistocene clastic sediment. These ranged in volume from a fraction of a cubic metre to a few hundred thousand cubic metres. They found

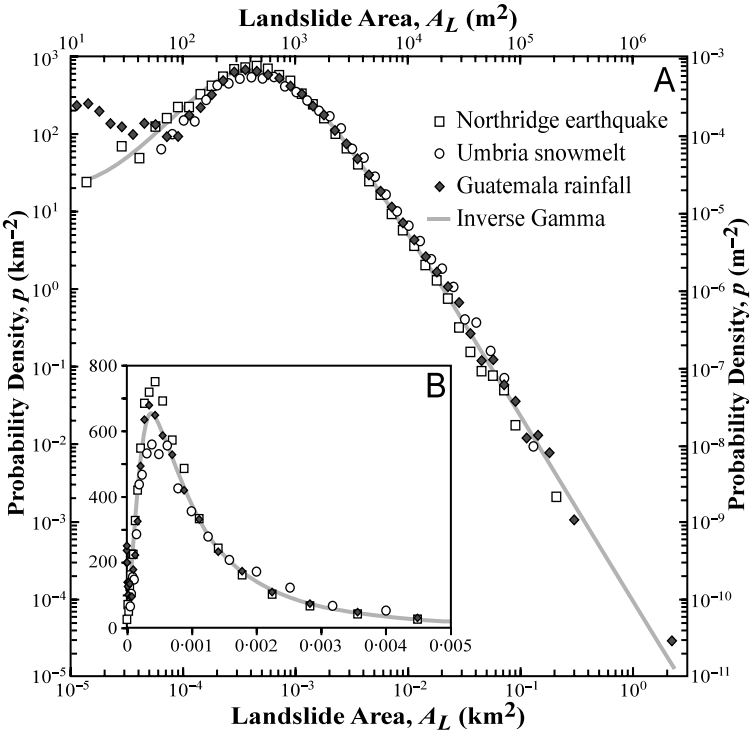

Figure 1. Dependence of landslide probability densities p on landslide area A_L, for three landslide inventories: (1) 11 111 landslides triggered by the 17 January 1994 Northridge earthquake in California, USA (open squares) (Harp and Jibson, 1995, 1996); (2) 4233 landslides triggered by a snowmelt event in the Umbria region of Italy in January 1997 (open circles) (Cardinali *et al*., 2000); (3) 9594 landslides triggered by heavy rainfall from Hurricane Mitch in Guatemala in late October and early November 1998 (closed diamonds) (Bucknam *et al*., 2001). Probability densities are given on logarithmic axes (**A**) and linear axes (**B**). Also included is our proposed landslide probability distribution. This is the best fit to the three landslide inventories of the three-parameter inverse-gamma distribution (Equation 3), with parameter values $\rho = 1{\cdot}40$, $a = 1{\cdot}28 \times 10^{-3}$ km^2, $s = -1{\cdot}32 \times 10^{-4}$ km^2

that deep-seated (>5 m) rotational slumps and block slides were far fewer in number but contributed significantly to the total landslide volume. The largest failure was a block slide with volume 8×10^6 m^3. The probability densities of landslide areas triggered by the Northridge earthquake are given in Figure 1 (open squares) as a linear–linear plot in Figure 1B and as a log–log plot in Figure 1A.

Our second example is an inventory of landslides in the Umbria region of central Italy that were triggered by a snowmelt event following a sudden change in temperature on 1 January 1997. Cardinali *et al*. (2000) compiled the inventory, covering an area of about 2000 km^2, through extensive field reconnaissance carried out in the weeks immediately after the event, and through the analysis of aerial photographs flown three months after the event at a nominal scale 1:120 000. The inventory contains 4233 landslides, for a total landslide area of 12·7 km^2 (0·6 per cent of the study area), with an average density of about 2·1 landslides per square kilometre. Snowmelt-triggered slope failures were mostly shallow soil-slips (53 per cent of the total number), and slump earth-flows (9 per cent), but also included deep-seated failures (38 per cent) which comprised complex or compound movements. The majority of the failures involved Plio-Pleistocene lake and marine clay and silt, and subordinately Tertiary marine clastic sediments. The probability densities of landslide areas triggered by the snowmelt event in Umbria are also given in Figure 1 (open circles).

Our third example is an inventory of landslides in Guatemala that were triggered by heavy rainfall from Hurricane Mitch in late October and early November 1998. Bucknam *et al*. (2001) mapped the landslides from 1:40 000-scale aerial photographs, covering an area of about 10 000 km^2. The inventory contains 9594 landslides, chiefly soil slips, debris flows and a few complex, deep-seated slides, with landslides occurring mostly in Holocene colluvial soil, Permian siltstone, Quaternary volcanic rocks, and Palaeozoic phyllite and

schist. We have omitted from their inventory 277 landslides with length-to-width ratios >50. We believe these represent very long low-density debris flows – hyperconcentrated streamflows (Pierson and Costa, 1987) – along the floors of the valleys, with their applicable physics more closely representing floods than the other landslides considered. The total landslide area in the inventory is 29·5 km^2 (0·3 per cent of the study area) with an average density of about 1·0 landslide per square kilometre. The probability densities of landslide areas triggered by Hurricane Mitch in Guatemala are shown in Figure 1 (closed diamonds).

The three distributions are in remarkably good agreement with each other. We have chosen these three data sets because there is strong evidence that they are substantially complete so that the rollover at small areas is well documented. The three studies were carried out within hours to a couple of months of the landslide events. Therefore, wasting processes did not obliterate smaller landslides and the boundaries of even small landslides were distinct. For the Northridge earthquake, Umbria snowmelt, and Guatemala heavy-rainfall landslide inventories, the authors (Harp and Jibson, 1995; Cardinali *et al*., 2000; Bucknam *et al*., 2001) estimated that their inventories are nearly complete for landslides with length scales greater than 5 m ($A_L \approx 25$ m^2), 15 m ($A_L \approx 225$ m^2), and 15 m ($A_L \approx 225$ m^2), respectively. The deviation from the rollover of the Guatemala data for landslide areas $A_L < 80$ m^2 may be attributed to the fact that these areas are below the resolution limit.

While some small landslides were undoubtedly omitted from the inventories, the landslides have been consistently mapped below the size of the most abundant landslide, $A_L \approx 400$ m^2 in Figure 1, thus indicating that this rollover (inflection) for small landslides is real. If the rollover were an artefact, there would be very large numbers of small landslides in nature. Field evidence from many regions suggests that the required large numbers of small landslides do not exist. We conclude that the rollover of the distribution for small landslides is real and not an artefact of inventory resolution. Therefore, a complete probability distribution can be defined.

We correlate the three sets of landslide probability densities given in Figure 1 with the three-parameter inverse-gamma probability distribution (Johnson and Kotz, 1970; Evans *et al*., 2000):

$$p(A_L;\, \rho, a, s) = \frac{1}{a\Gamma(\rho)}\left[\frac{a}{A_L - s}\right]^{\rho+1} \exp\left[-\frac{a}{A_L - s}\right] \tag{3}$$

where $\Gamma(\rho)$ is the gamma function of ρ. The inverse-gamma distribution $f(y)$ is obtained by making the substitution $x = 1/y$ into the gamma distribution $f(x)$, and is essentially an inverse power-law decay for medium and large areas, and an exponential rollover for small areas. We selected the three-parameter inverse-gamma distribution because a comparative test of over 300 statistical distributions showed that it provided the best fit. As the probability densities span seven orders of magnitude and the landslide areas five orders, least-squares fitting was not appropriate and we used a robust (maximum likelihood) fitting algorithm based on Lorentzian minimization of the errors.

For large values of A_L, the inverse-gamma distribution given in Equation 3 can be approximated by

$$p(A_L) \approx \frac{1}{a\Gamma(\rho)}\left[\frac{a}{A_L}\right]^{\rho+1} \tag{4}$$

The tail of the probability distribution for large landslide areas is a power-law (a 'fat-tailed' distribution) with exponent $-(\rho + 1)$. The parameter ρ (Equations 3 and 4) controls the power-law decay for medium and large landslide areas, the parameter a (Equation 3) primarily controls the location of the maximum probability distribution, and the parameter s (Equation 3) primarily controls the exponential decay for small landslide areas. The maximum-likelihood fit of the inverse-gamma distribution (Equation 3) to the three sets of landslide probability densities given in Figure 1 is obtained taking $\rho = 1{\cdot}40$, $a = 1{\cdot}28 \times 10^{-3}$ km^2, and $s = -1{\cdot}32 \times 10^{-4}$ km^2 ($\Gamma(1{\cdot}4) = 0{\cdot}88726$); for this fit we have $r^2 = 0{\cdot}965$.

We find a value of $\rho + 1 \approx 2{\cdot}4$ for the power-law tail of our proposed landslide distribution. In their study, Stark and Hovius (2001) correlated their probability densities of landslides with a double Pareto distribution, which also has a power-law tail for large landslides. Their equivalent values for $\rho + 1$ were 2·11 for medium and large landslides in Taiwan and 2·44 and 2·48 for medium and large landslides in New Zealand.

It should be noted that the integral of the inverse-gamma distribution given in Equation 3 is normalized to 1 over the interval $s \le A_L < \infty$, where in our case s has a negative value. This normalization condition requires

$$\int_s^{\infty} \frac{1}{a\Gamma(\rho)} \left[\frac{a}{A_L - s}\right]^{\rho+1} \exp\left[-\frac{a}{A_L - s}\right] dA_L = 1 \tag{5}$$

However, our distribution of landslides is defined over the interval $0 \le A_L < \infty$. Thus, an error is introduced in the left-hand side of Equation 5, over the interval $s \le A_L \le 0$. We will now show that this error is negligible. We can write

$$\begin{aligned} &\int_0^{\infty} \frac{1}{a\Gamma(\rho)} \left[\frac{a}{A_L - s}\right]^{\rho+1} \exp\left[-\frac{a}{A_L - s}\right] dA_L = \\ &\int_s^{\infty} \frac{1}{a\Gamma(\rho)} \left[\frac{a}{A_L - s}\right]^{\rho+1} \exp\left[-\frac{a}{A_L - s}\right] dA_L - \int_s^{0} \frac{1}{a\Gamma(\rho)} \left[\frac{a}{A_L - s}\right]^{\rho+1} \exp\left[-\frac{a}{A_L - s}\right] dA_L \end{aligned} \tag{6}$$

The definition of the incomplete gamma function (Abramowitz and Segun, 1965, p. 260) is

$$\Gamma(\rho, -a/s) = \int_{-a/s}^{\infty} y^{\rho-1} \exp(-y)\, dy \tag{7}$$

Substitution of $y = a/(A_L - s)$ and $dy = -a dA_L/(A_L - s)^2$ in Equation 7, appropriately changing the limits, and dividing both sides of the equation by $\Gamma(\rho)$ gives

$$\frac{\Gamma(\rho, -a/s)}{\Gamma(\rho)} = \frac{1}{\Gamma(\rho)} \int_s^{0} \frac{1}{a} \left[\frac{a}{A_L - s}\right]^{\rho+1} \exp\left[-\frac{a}{A_L - s}\right] dA_L \tag{8}$$

Substitution of Equations 5 and 8 into the right-hand side of Equation 6 gives

$$\int_0^{\infty} \frac{1}{a\Gamma(\rho)} \left[\frac{a}{A_L - s}\right]^{\rho+1} \exp\left[-\frac{a}{A_L - s}\right] dA_L = 1 - \frac{\Gamma(\rho, -a/s)}{\Gamma(\rho)} \tag{9}$$

The term $\Gamma(\rho, -a/s)/\Gamma(\rho)$ is the correction. However, when $-a/s$ is large we have the approximate relation (Abramowitz and Segun, 1965, p. 263)

$$\Gamma\left(\rho, -\frac{a}{s}\right) = \left(-\frac{a}{s}\right)^{\rho-1} \exp\left(\frac{a}{s}\right) \tag{10}$$

For our best-fit distribution given in Figure 1, we have $\rho = 1{\cdot}40$ and $-a/s = 9{\cdot}70$, so that the correction term $\Gamma(\rho, -a/s)/\Gamma(\rho) = 0{\cdot}000152/0{\cdot}88726 \approx 10^{-4}$. Thus we can neglect the correction in Equation 9 given by $\Gamma(\rho, -a/s)/\Gamma(\rho)$; integrating Equation 3, our probability density distribution over $s \le A_L < \infty$, is for our purposes identical to integrating over $0 \le A_L < \infty$.

Based on the excellent agreement between the three landslide inventories and our best-fit three-parameter inverse-gamma distribution illustrated in Figure 1, we hypothesize that our best-fit distribution is a 'general' landslide distribution. We do not expect all landslide-event inventories to be in as good agreement as the three we have considered, but we do argue that the quantification, if only approximate, will be valuable in assessing the landslide hazard.

MEAN LANDSLIDE AREA

Assuming the validity of Equation 3 for the probability distribution of landslide areas in individual landslide events, we can use this distribution to derive a theoretical mean landslide area $\bar{A}_L$. This is the mean of all landslide areas that occur during a landslide event. The theoretical mean area is obtained by taking the first moment of the probability density function, giving

$$\bar{A}_L = \int_0^\infty A_L p(A_L) dA_L \tag{11}$$

Substituting the three-parameter inverse-gamma distribution from Equation 3 into Equation 11 and simplifying gives

$$\begin{aligned}
\bar{A}_L &= \frac{1}{a\Gamma(\rho)} \int_0^\infty A_L \left[\frac{a}{A_L - s}\right]^{\rho+1} \exp\left[-\frac{a}{A_L - s}\right] dA_L \\
&= \frac{1}{\Gamma(\rho)} \int_0^\infty \left[\frac{A_L - s}{a}\right] \left[\frac{a}{A_L - s}\right]^{\rho+1} \exp\left[-\frac{a}{A_L - s}\right] dA_L + s \int_0^\infty \frac{1}{a\Gamma(\rho)} \left[\frac{a}{A_L - s}\right]^{\rho+1} \exp\left[-\frac{a}{A_L - s}\right] dA_L \\
&= \frac{1}{\Gamma(\rho)} \int_0^\infty \left[\frac{a}{A_L - s}\right]^{\rho} \exp\left[-\frac{a}{A_L - s}\right] dA_L + s
\end{aligned} \tag{12}$$

In Equation 12, we have used the integral given in Equation 9, with, as discussed after Equation 10, $\Gamma(\rho, -a/s)/\Gamma(\rho)$ set to 0. Again making the substitution $y = a/(A_L - s)$ and $dA_L = -ady/y^2$, Equation 12 becomes

$$\begin{aligned}
\bar{A}_L &= \frac{a}{\Gamma(\rho)} \int_0^{-a/s} y^{\rho-2} \exp(-y) dy + s \\
&\approx \frac{a}{\Gamma(\rho)} \int_0^\infty y^{\rho-2} \exp(-y) dy + s
\end{aligned} \tag{13}$$

where the upper limit of integration $-a/s$ has been replaced by infinity since we have $-a/s = 9{\cdot}70$ for our distribution and $\exp(-9{\cdot}7) \approx 0$. The definite integral in Equation 13 is the gamma function $\Gamma(\rho - 1)$ which is equal to $\Gamma(\rho)/(\rho - 1)$, so that we have

$$\bar{A}_L = \frac{a}{\rho - 1} + s \tag{14}$$

For the landslide probability distribution given in Figure 1 we have $a = 1{\cdot}28 \times 10^{-3}$ km^2, $s = -1{\cdot}32 \times 10^{-4}$ km^2 and $\rho = 1{\cdot}40$, so that $\bar{A}_L = 3{\cdot}07 \times 10^{-3}$ km^2. One implication of our landslide distribution is that since the probability distribution always has the same mean, then all landslide events should have the same mean landslide area $\bar{A}_L = 3{\cdot}07 \times 10^{-3}$ km^2 = 3070 m^2. This follows directly from the applicability of our proposed landslide distribution, and is independent of the number of landslides associated with a landslide event. The measured mean landslide areas $\bar{A}_L$ for the three event inventories, Umbria, Northridge and Guatemala, are $\bar{A}_L = 3{\cdot}01 \times 10^{-3}$ km^2, $2{\cdot}14 \times 10^{-3}$ km^2, and $3{\cdot}07 \times 10^{-3}$ km^2, in good agreement with the value predicted by our distribution (see Table II).

TOTAL LANDSLIDE AREA

When examining landslides associated with individual landslide events, we are often interested in knowing A_{LT}, the total area of *all* landslides that occurred as part of the event. Using the theoretical mean landslide area $\bar{A}_L$ from Equation 14, and the number of landslides that occur during the event, we can calculate a predicted total area A_{LT} of landslides in the inventory.

If N_{LT} is the total number of landslides in a complete inventory, then the predicted total area of the landslides in the inventory is

$$A_{LT} = N_{LT}\bar{A}_L = \left(\frac{a}{\rho - 1} + s\right)N_{LT} = 3{\cdot}07 \times 10^{-3} N_{LT} \tag{15}$$

with A_{LT} in km^2. Using Equation 15 and N_{LT}, we find predicted total areas $A_{LT} = 13{\cdot}0$, $34{\cdot}1$, and $30{\cdot}6$ km^2 for Umbria, Northridge and Guatemala respectively. This compares with the actual inventory values of $A_{LT} = 12{\cdot}7$, $23{\cdot}8$ and $29{\cdot}5$ km^2, respectively (see Table II).

We can also use our landslide distribution to extrapolate a partial inventory of landslide areas to give the total landslide area A_{LT}. Let $A_{LC}(\geq A_L)$ be the cumulative area of all landslides in a partial inventory with areas $\geq A_L$. We now derive a relationship between this cumulative area $A_{LC}(\geq A_L)$ and the total area A_{LT}.

Substituting Equation 11 into Equation 15, and changing the lower limit of integration from 0 to A_L, the cumulative area $A_{LC}(\geq A_L)$ is given by

$$A_{LC}(\geq A_L) = N_{LT}\int_{A_L}^{\infty} A_L p(A_L) dA_L \tag{16}$$

with N_{LT} the total number of landslides that occurred during the landslide event. Substituting the three-parameter inverse-gamma distribution from Equation 3 into Equation 16, we obtain

$$A_{LC}(\geq A_L) = \frac{N_{LT}}{a\Gamma(\rho)}\int_{A_L}^{\infty}\left[\frac{a}{A_L - s}\right]^{\rho+1}\exp\left[-\frac{a}{A_L - s}\right]A_L dA_L \tag{17}$$

We have integrated this equation numerically using parameter values corresponding to the distribution given in Figure 1. The resulting dependence of the ratio $A_{LC}(\geq A_L)/A_{LT}$ on A_L is given in Figure 2. For instance, assume that the areas of all landslides with areas $A_L \geq 0{\cdot}1$ km^2 have been determined. From Figure 2 we see that the ratio $A_{LC}(\geq 0{\cdot}1 \text{ km}^2)/A_{LT} = 0{\cdot}2$, or that the cumulative area represents 20 per cent of the total landslide area, so $A_{LC}(\geq 0{\cdot}1 \text{ km}^2)$ can be multiplied by five to estimate the total landslide area A_{LT} for the substantially complete inventory.

As an example, consider the three landslide inventories in Figure 1, and what would happen if each were only a 'partial' inventory. In Table III, we give landslide areas A_L in the first two columns and values for the ratio $A_{LC}(\geq A_L)/A_{LT}$ from Figure 2 (Equation 17) in the third column. We then give $N_{LC}(\geq A_L)$, the number of landslides with areas $\geq A_L$ (A_L from the first two columns), $A_{LC}(\geq A_L)$, the actual cumulative area of all measured landslides in the 'partial' inventory with areas $\geq A_L$, and finally the predicted value of A_{LT} using the theoretical ratio of $A_{LC}(\geq A_L)/A_{LT}$ and the measured partial inventory $A_{LC}(\geq A_L)$.

For instance, consider an estimate of the total landslide area in the Umbria snowmelt inventory using about 10 per cent of the landslides. For this inventory, 394 landslides (9·3 per cent of the total) have areas $A_{LC} \geq 6{\cdot}31 \times 10^{-3}$ km^2, with partial inventory area $A_{LC}(\geq 6{\cdot}31 \times 10^{-3} \text{ km}^2) = 6{\cdot}72$ km^2. The theoretical ratio $A_{LC}(\geq 6{\cdot}31 \times 10^{-3} \text{ km}^2)/A_{LT} = 0{\cdot}584$, so based only on the largest 9·3 per cent of the inventory, we estimate the total landslide area to be $A_{LC} = 11{\cdot}51$ km^2. The actual total area for the complete inventory is $A_{LC} = 12{\cdot}73$ km^2, approximately 10 per cent different. For the Northridge, Umbria and Guatemala inventories (Table III), using just the 10 per cent largest landslides, our theoretical estimate for the total landslide areas gives 82, 90 and 99 per cent of the actual total landslide areas. If an inventory of landslides associated with a trigger is complete for just the largest landslides that have occurred during the event, the total area of *all* landslides that have occurred during the event can be determined. Similarly, using just the areas of the largest landslides, we can estimate the total number of landslides that have occurred during the event. This will be discussed in more detail in a later section.

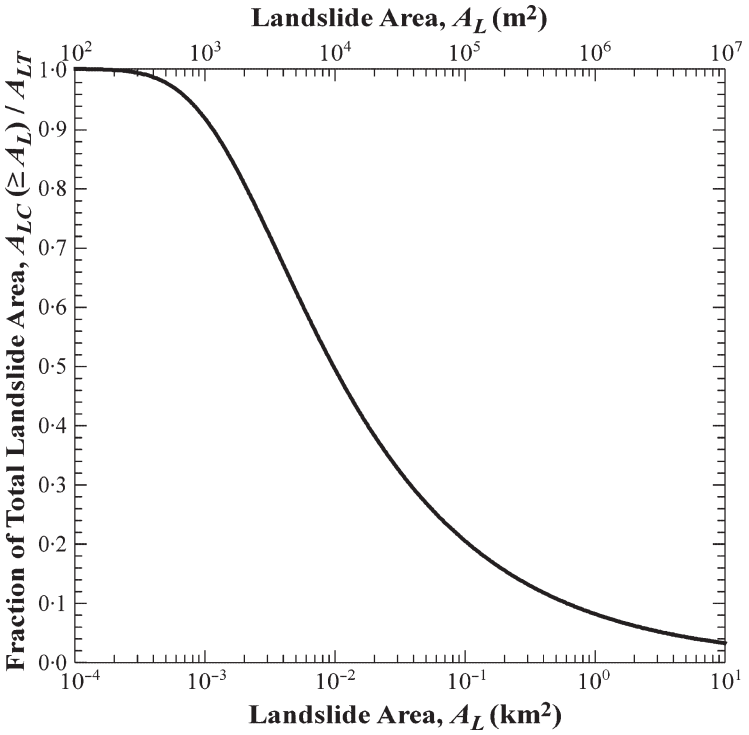

Figure 2. Dependence of the ratio $A_{LC}(\geq A_L)/A_{LT}$ on A_L, where $A_{LC}(\geq A_L)$ is the cumulative area of landslides in a landslide event with areas greater than or equal to landslide area A_L, and A_{LT} is the total of all landslide areas in the event. The ratio $A_{LC}(\geq A_L)/A_{LT}$ is given on linear axes and the landslide area on logarithmic axes. The dependence of $A_{LC}(\geq A_L)/A_{LT}$ on A_L is obtained from integrating Equation 17 numerically using parameter values from Figure 1 corresponding to the landslide probability distribution, Equation 3

FREQUENCY–VOLUME DISTRIBUTIONS

Volume is another measure of the size of a landslide. Volumes are much more difficult to measure than areas, as areas can be obtained from aerial photographs, but volumes generally cannot. For this reason, landslide distributions are generally given in terms of areas. Landslide volumes are of particular interest because they can be related to erosion rates.

Simonett (1967) utilized field studies to obtain the volumes and areas of 201 landslides in the Bewani and Torricelli Mountains, New Guinea. He correlated his results with the power-law relation

$$V_L = 0{\cdot}024 A_L^{1{\cdot}368} \tag{18}$$

with landslide area A_L in km^2 and landslide volume V_L in km^3. Hovius *et al*. (1997) have also studied this problem and they suggested the relation

$$V_L = \varepsilon A_L^{1{\cdot}50} \tag{19}$$

with $\varepsilon = 0{\cdot}05 \pm 0{\cdot}02$. We have used both relations to determine the volume of each landslide in the three inventories considered above. The volumes within each inventory were then added to obtain the total and mean landslide volumes for the three landslide events. The results, using Equations 18 and 19, are presented in Table II. While the mean areas for the three inventories are nearly equal, the mean volumes for the Guatemala rainfall inventory are considerably larger than for the other two inventories. As we will show, the mean volumes are sensitive to the largest landslides, whereas the mean areas are less sensitive. Since the differences between the two empirical correlations, Equations 18 and 19, are relatively small, we will utilize Equation 19 in our further analyses. Clearly, any correlation is approximate and may vary with landslide type and size.

Table III. Predictions of landslide event total landslide areas A_{LT} based on partial inventories

		Theory*	Northridge earthquake†‡			Umbria snowmelt†§			Guatemala rainfall†¶		
A_L (km^2)	A_L (m^2)	$\frac{A_{LC}(\geq A_L)}{A_{LT}}$	N_{LC} ($\geq A_L$)	$A_{LC}(\geq A_L)$ (km^2)	A_{LT} (km^2)	N_{LC} ($\geq A_L$)	$A_{LC}(\geq A_L)$ (km^2)	A_{LT} (km^2)	N_{LC} ($\geq A_L$)	$A_{LC}(\geq A_L)$ (km^2)	A_{LT} (km^2)
0·100	100 000	0·207	6	0·90	4·35	4	0·48	2·32	14	5·83	28·22
0·0631	63 100	0·248	19	1·85	7·49	10	0·89	3·58	30	7·06	28·51
0·0398	39 800	0·297	40	2·89	9·74	29	1·76	5·93	57	8·41	28·36
0·0251	25 100	0·354	77	4·02	11·34	61	2·75	7·77	120	10·28	29·03
0·0158	15 800	0·421	179	6·00	14·23	137	4·26	10·11	237	12·59	29·87
0·0100	10 000	0·498	357	8·18	16·41	236	5·48	11·00	413	14·78	29·66
0·00631	6 310	0·584	657	10·52	18·01	394	6·72	11·51	733	17·30	29·62
0·00398	3 980	0·676	1 177	13·12	19·40	687	8·18	12·10	1258	19·90	29·44
0·00251	2 510	0·768	2 019	15·75	20·50	1158	9·66	12·57	2094	22·53	29·32
0·00158	1 580	0·852	3 327	18·34	21·51	1795	10·92	12·81	3334	24·98	29·31
0·00100	1 000	0·919	5 155	20·64	22·45	2448	11·75	12·78	4920	26·98	29·34
0·000631	631	0·964	7 300	22·36	23·20	3154	12·31	12·78	6619	28·34	29·40
0·000398	398	0·987	9 155	23·31	23·62	3686	12·59	12·75	8028	29·05	29·43
0·000251	251	0·996	10 302	23·69	23·77	4009	12·69	12·74	8983	29·36	29·47
0·000158	158	0·999	10 807	23·79	23·81	4165	12·73	12·74	9365	29·44	29·47
0·000100	100	1·000	10 989	23·82	23·82	4213	12·73	12·73	9481	29·46	29·46
Inventory totals			**11 111**		**23·83**	**4233**		**12·73**	**9594**		**29·46**

* $A_{LC}(\geq A_L)$ is the cumulative area of inventory landslides with areas $\geq A_L$, with A_{LT} the total of landslide areas in the 'complete' inventory. The theoretical ratios $A_{LC}(\geq A_L)/A_{LT}$ are obtained from Equation 17 and Figure 2, and are given for various landslide areas A_L.

† Measured values of the cumulative number of landslides $N_{LC}(\geq A_L)$ and the cumulative areas of landslides $A_{LC}(\geq A_L)$ with areas greater than A_L, are given for the three landslide inventories in Figure 1. The predicted 'complete' inventory total area A_{LT} is based on the 'partial' inventory $A_{LC}(\geq A_L)$ and the theoretical ratio $A_{LC}(\geq A_L)/A_{LT}$.

‡ Landslides triggered by earthquake, 17 January 1994, Northridge, California, USA (Harp and Jibson, 1995, 1996).

§ Landslides triggered by rapid snowmelt, January 1997, Umbria, Italy (Cardinali *et al*., 2000; Guzzetti *et al*., 2002).

¶ Landslides triggered by heavy rainfall from Hurricane Mitch, late October/early November, 1998, Guatemala (Bucknam *et al*., 2001).

We will now derive a mean landslide volume $\bar{V}_L$ from our landslide distribution. Using Equation 1, we can write the mean landslide volume $\bar{V}_L$ as

$$\bar{V}_L = \frac{V_{LT}}{N_{LT}} = \frac{\int_0^\infty V_L dN_L}{N_{LT}} = \frac{\int_0^\infty V_L \left(\frac{dN_L}{dA_L}\right) dA_L}{N_{LT}} = \frac{\int_0^\infty V_L (N_{LT}\, p(A_L)) dA_L}{N_{LT}} = \int_0^\infty V_L p(A_L) dA_L \tag{20}$$

Assuming the validity of Equation 19, and substituting it into Equation 20, then

$$\bar{V}_L = \varepsilon \int_0^\infty A_L^{1{\cdot}50} p(A_L) dA_L \tag{21}$$

Substitution of Equation 3 for $p(A_L)$, assuming s can be neglected when compared with A_L, and letting $x = A_L/a$, we have

$$\bar{V}_L = \frac{\varepsilon a^{1{\cdot}50}}{\Gamma(\rho)} \int_0^\infty \frac{1}{x^{\rho - 0{\cdot}5}} \exp\left[-\frac{1}{x}\right] dx \tag{22}$$

Unfortunately, for ρ less than 1·5, this integral diverges for large area landslides. Since we find $\rho = 1{\cdot}40$ for our landslide distribution, we must prescribe a largest landslide in order to obtain a finite mean landslide volume. Taking the maximum landslide area to be $A_{L\max}$, integration of Equation 22 numerically gives

$$\bar{V}_L = \frac{\varepsilon a^{1{\cdot}50}}{\Gamma(\rho)}\left[\frac{1}{(1{\cdot}50-\rho)}\left(\frac{A_{L\max}}{a}\right)^{1{\cdot}50-\rho} - 10{\cdot}69\right] \tag{23}$$

In order to specify $A_{L\max}$ we determine the largest landslide that can be expected in a landslide event. Utilizing the definition of the probability density (Equation 1) and the landslide probability distribution for landslides with large areas (Equation 4), then $N_{LC}(\geq A_L)$, the cumulative number of landslides with areas $\geq A_L$, is given by

$$N_{LC}(\geq A_L) = \int_{A_L}^{\infty} dN_L = \int_{A_L}^{\infty} N_{LT}\, p(A_L)\, dA_L = \frac{N_{LT}}{a\Gamma(\rho)}\int_{A_L}^{\infty}\left(\frac{a}{A_L}\right)^{\rho+1} dA_L = \frac{N_{LT}}{\rho\Gamma(\rho)}\left(\frac{a}{A_L}\right)^{\rho} \tag{24}$$

We define $A_{L\max}$ the largest landslide to be the landslide corresponding to $N_{LC}(\geq A_L) = 1$ so that

$$A_{L\max} = a\left(\frac{N_{LT}}{\rho\Gamma(\rho)}\right)^{\frac{1}{\rho}} \tag{25}$$

For the landslide distribution given in Figure 1 we have $a = 1{\cdot}28 \times 10^{-3}$ km^2, $\rho = 1{\cdot}40$, and $\Gamma(\rho) = 0{\cdot}88726$ so that

$$A_{L\max} = 1{\cdot}10 \times 10^{-3}\ N_{LT}^{0{\cdot}714} \tag{26}$$

with $A_{L\max}$ in km^2. We compare (see Table II) this predicted largest landslide area with the actual largest landslide areas for the three inventories we have considered. There is a factor of 3–5 statistical scatter for the largest landslides in each inventory. This is reasonable considering the tail of the distribution involves very few data values.

Using the relationship between landslide volume and area given in Equation 19, with $\varepsilon = 0.05$, we can substitute $A_{L\max}$ from Equation 26 and obtain an expression for $V_{L\max}$, the largest landslide volume in a landslide event

$$V_{L\max} = 1{\cdot}82 \times 10^{-6}\ N_{LT}^{1{\cdot}071} \tag{27}$$

with $V_{L\max}$ in km^3.

We return now to our determination of $\bar{V}_L$, the mean landslide volume in a landslide event. Substitution of Equation 25 into Equation 23 gives $\bar{V}_L$ as a function of the total number of landslides

$$\bar{V}_L = \frac{\varepsilon a^{1{\cdot}50}}{\Gamma(\rho)}\left[\frac{1}{(1{\cdot}50-\rho)}\left(\frac{N_{LT}}{\rho\Gamma(\rho)}\right)^{\frac{1{\cdot}50-\rho}{\rho}} - 10{\cdot}69\right] \tag{28}$$

Substituting $\varepsilon = 0{\cdot}05$ and the landslide distribution values given in Figure 1, $a = 1{\cdot}28 \times 10^{-3}$ km^2, $\rho = 1{\cdot}40$, and $\Gamma(\rho) = 0{\cdot}88726$, we have

$$\bar{V}_L = 2{\cdot}58 \times 10^{-6}\ (9{\cdot}85 N_{LT}^{0{\cdot}0714} - 10{\cdot}69) \tag{29}$$

The dependence of $\bar{V}_L$ on N_{LT} is given in Figure 3, using logarithmic axes. Also given in this figure is the best-fit straight line (power law) over the range $N_{LT} = 10^4$ to 10^8. This best fit is given by

$$\bar{V}_L = 7{\cdot}30 \times 10^{-6}\ N_{LT}^{0{\cdot}1222} \tag{30}$$

with $\bar{V}_L$ in km^3 and $r^2 = 0{\cdot}996$. We will use this approximate power-law fit in the next section.

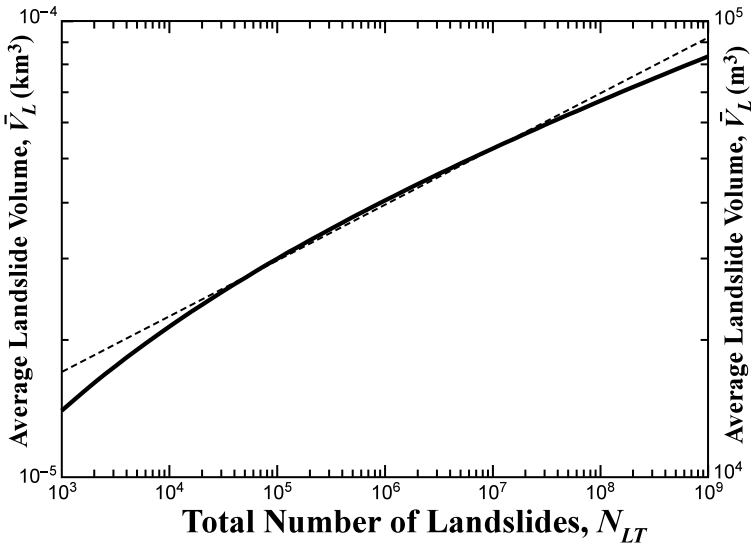

Figure 3. Dependence of the mean landslide volume in a landslide event $\bar{V}_L$ on the total number of landslides in the event N_{LT}, both on logarithmic axes. The solid line is from Equation 28 and the dashed line is the straight line best fit given by the power-law Equation 30. This is the best-fit (power-law) straight line over the range $N_{LT} = 10^4$ to 10^8

In Table II, we have compared mean landslide volumes calculated using Equations 18 and 19 (conversions of actual areas to volumes) with predicted volumes from Equation 30. Again, there is scatter (about a factor of 2), due to the largest landslides dominating total landslide volume, and scatter in the sizes of these largest landslides.

LANDSLIDE-EVENT MAGNITUDE SCALE

Measures of landslide event sizes are useful for natural hazards. For example, the Richter magnitude scale for earthquakes is universally used and the general public has some understanding of the implications of an $M = 7{\cdot}5$ earthquake. The magnitude of an earthquake is determined from the strength of the associated seismic waves. The magnitude is proportional to the logarithm (base 10) of the energy in the waves. There are several alternative definitions of earthquake magnitude and all are approximate due to the many complexities involved. Errors in magnitude estimation are generally at least 5 per cent, or about a factor of three error in the energy of the waves. Nevertheless, even this approximate measure of earthquake amplitude is useful because the energy ranges over many orders of magnitude. Over a dozen magnitude scales are available for other natural hazards, including the Saffir–Simpson scale (hurricanes), the Fujita scale (tornadoes), and the Volcanic Explosivity Index.

We propose that an appropriate magnitude scale m_L for a landslide event is the logarithm to the base 10 of the total number of landslides associated with the event:

$$m_L = \log N_{LT} \tag{31}$$

Keefer (1984) has used a similar scale to quantify the number of landslides in earthquake-triggered landslide events: 100–1000 landslides were classified as a two, 1000–10 000 landslides a three, etc. If a substantially complete inventory of the landslides in an event has been carried out, then the event magnitude is easily obtained.

The total measured area of landslides associated with a landslide event A_{LT} can also be used to determine the landslide magnitude m_L. Assuming the applicability of our landslide distribution, we can combine Equations 15 and 31 to give

$$m_L = \log A_{LT} + 2{\cdot}51 \tag{32}$$

with A_{LT} in km^2.

Using Equations 31 and 32, the landslide magnitudes for the three landslide events that we have considered are given in Table II, and vary in the range $m_L = 3{\cdot}6 - 4{\cdot}0$. For these examples, using the total area of landslides or the total number of landslides gives very similar magnitudes, less than 4 per cent different.

The total measured volume of landslides associated with a landslide event V_{LT} can also be used to determine the landslide magnitude m_L. From Equation 30 we have

$$V_{LT} = \bar{V}_L N_{LT} = 7{\cdot}30 \times 10^{-6}\ N_{LT}^{1{\cdot}1222} \tag{33}$$

with $\bar{V}_L$ and V_{LT} in km^3. Combining Equations 31 and 33 we have

$$m_L = 0{\cdot}89 \log V_{LT} + 4{\cdot}58 \tag{34}$$

with V_{LT} in km^3. The predicted total landslide area (Equation 15), largest landslide area (Equation 26), total landslide volume (Equation 33), and largest landslide volume (Equation 27) are given in Figure 4 as a function of landslide-event magnitude and total number of landslides in the event. This graph allows us to relate the total volume of mass wasting to the landslide-event magnitude and make estimates of the largest landslide associated with a given magnitude landslide event.

While observed earthquakes span a wide range on the Richter scale, available landslide-event inventories are restricted to a relatively narrow magnitude range, approximately $m_L = 3 - 4$. There are several reasons for this. Accurate inventories are restricted to populated areas and have been carried out only during the last ten years or so. Thus, very few large landslide events with $m_L > 4$ have occurred in regions where studies have been carried out. In addition, there has been little incentive to carry out studies of small magnitude landslide events,

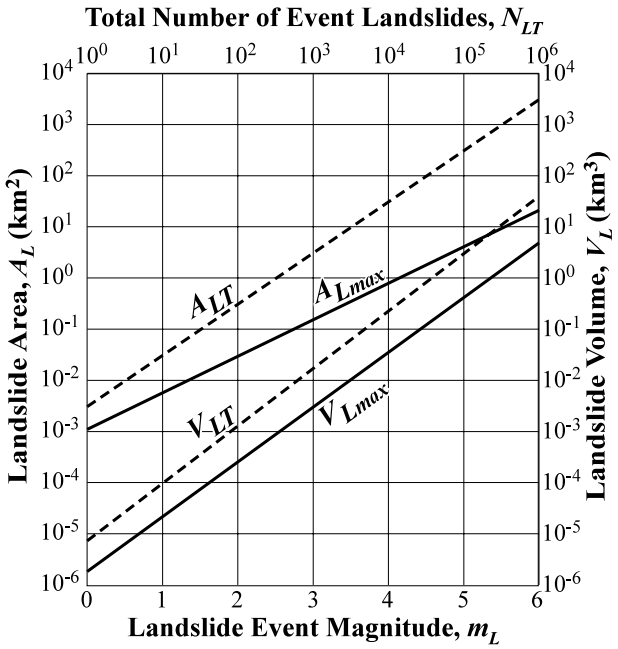

Figure 4. Predicted landslide-event areas and volumes associated with a given landslide-event magnitude. The predicted total landslide area A_{LT} (dashed line) from Equation 15, the largest landslide area A_{Lmax} (solid line) from Equation 26, the total landslide volume V_{LT} (dashed line) from Equation 33, and the largest landslide volume V_{Lmax} (solid line) from Equation 27 are given as a function of landslide-event magnitude m_L defined in Equation 31 and total number of landslides N_{LT} in an event. The variables A_L, N_{LT}, and V_L are given on logarithmic axes, and m_L on linear axes

Table IV. Historical (regional) landslide inventories

Location*	Landslides ages†	Inventory N_{LT}‡	m_L§	Over time N_{LT}¶	Total landslides 'lost' (%)◇
Ma–An and Wan–Li catchments, Taiwan	<10 y	1040	3·3 ± 0·1	2050 ± 450	47 ± 12
Challana Valley, Bolivia	<10–25 y	1131	3·6 ± 0·1	4100 ± 900	71 ± 6
Umbria, Italy	<5–10 ky	A: 5288 B: 44 724	5·8 ± 0·1	650 000 ± 150 000	A: 99·1 ± 0·2 B: 92·7 ± 1·7
Akaishi Ranges, Japan	<10 ky	3424	6·0 ± 0·2	1·1 ± 0·5 million	99·6 ± 0·2

* Hovius *et al*. (2000) – Taiwan; Pelletier *et al*. (1997) – Bolivia; Guzzetti *et al*. (2002) – Italy; Ohmori and Sugai (1995) – Japan.
† Landslide ages as estimated by respective authors, with y = years, and ky = thousands of years.
‡ Number of landslides in the historical landslide inventory.
§ Landslide-event magnitude, based on comparing the frequency densities of the medium and largest landslides to our inverse-gamma landslide distribution, Equation 3.
¶ Total number of landslides over time based on m_L.
◇ Percentage of landslides 'lost' over time due to erosion, vegetation growth, human activity, and landslide boundaries becoming less distinct.

$m_L = 1 - 3$. A limited range was also the case for earthquakes in the 1940s, when instrumental limitations limited studies to large earthquakes and the time span for studies was short so few large earthquakes had occurred.

INCOMPLETE LANDSLIDE INVENTORIES

Assuming that our landslide probability distribution is applicable, incomplete landslide inventories can be extrapolated to find the total area, total volume, and total number of landslides associated with a trigger. Incomplete landslide inventories include partial landslide-event inventories and historical inventories.

We will illustrate this extrapolation by considering several examples (see Table IV). In Figure 5, we give the frequency density of landslides $f = \delta N_L/\delta A_L$ as a function of A_L. We use frequency densities here since the inventories are incomplete and the normalization given in Equation 2 no longer holds. From Equation 1, we note that the frequency density is

$$f(A_L) = \frac{\delta N_L}{\delta A_L} = N_{LT} p(A_L) \tag{35}$$

Theoretical curves of $f(A_L)$ for various landslide-event magnitudes m_L can be obtained by multiplying the probability distribution $p(A_L)$ given in Equation 3 by the total number of landslides in the event N_{LT}. The parameter values are those given in Figure 1. Curves are given in Figure 5 for $m_L = 1$ ($N_{LT} = 10$) to $m_L = 8$ ($N_{LT} = 10^8$).

Included in Figure 5 are the frequency densities for five inventories. We include the three substantially complete landslide-event inventories previously given in Figure 1. As expected, these frequency densities are in relatively good agreement with the appropriate theoretical curve corresponding to the magnitude of the landslide event.

We also include in Figure 5 two historical inventories, with landslide ages <25 years. Due to the passage of time, it is unknown whether these inventories were the result of one landslide event or multiple events. The first inventory includes 1040 'fresh' landslides in the Ma–An and Wan–Li catchments in Taiwan given by Hovius *et al*. (2000). They estimated that the ages of these landslides were <10 years. The second inventory includes 1131 historical landslides in the Challana Valley, Eastern Cordillera, Bolivia (Pelletier *et al*., 1997). They estimated that the age of these landslides is <10–25 years. The two recent historical inventories still exhibit power-law tails with the same exponent $\rho + 1 \approx 2{\cdot}4$ as was found for our best fit to the three landslide-event inventories discussed previously. However, these inventories deviate from power-law behaviour at slightly larger landslide areas than the substantially complete event distributions.

Clearly, historical inventories cannot be attributed to a single landslide event. However, if individual landslide events that contributed to the historical inventories satisfy the landslide probability distribution given by

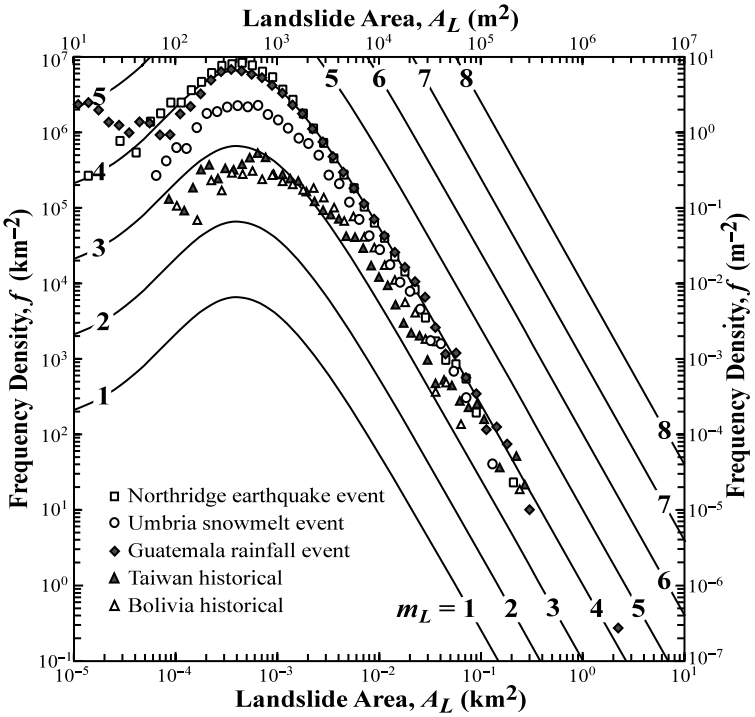

Figure 5. Dependence of the landslide frequency density f on landslide area A_L, both on logarithmic axes. Landslide frequency distributions corresponding to our proposed landslide probability distribution, Equations 3 and 35, are given for landslide magnitudes $m_L = 1, 2, \ldots, 8$ ($N_{LT} = 10, 10^2, \ldots, 10^8$). Also included are the frequency densities for five landslide inventories: the three 'complete' triggered event inventories given in Figure 1, Northridge earthquake (open squares), Umbria snowmelt (open circles), and Guatemala rainfall (closed diamonds); 1040 recent (<10 years) historical landslides in the Ma–An and Wan–Li catchments in Taiwan (closed triangles) (Hovius *et al*., 2000); and 1130 recent (10–25 years) historical landslides in the Challana Valley, Bolivia (open triangles) (Pelletier *et al*., 1997)

Equation 3, then the sum of events will also satisfy the distribution. The power-law behaviour of the historical distributions in Figure 6 is one potential confirmation of this superposition principle. Therefore, for the historical inventories, we attribute the deviation from our probability distribution to the incompleteness of the inventories. We argue that the evidence for the existence of the smaller landslides in these historical inventories has been lost due to erosion, human action, and vegetation, and that the landslide boundaries have become increasingly indistinct, making the landslides themselves harder to identify. We hypothesize that these inventories are complete for the large landslides and that our landslide event probability distribution is applicable to the historical inventories.

The results of this assumption are presented in Table IV for the two recent historical inventories. For the Taiwan inventory the power-law tail gives a landslide magnitude $m_L = 3{\cdot}3 \pm 0{\cdot}1$ so that $N_{LT} = 2050 \pm 450$ landslides. Since the number of landslides in the inventory is 1040, we conclude that the evidence for the existence of about 1000 ± 450 smaller landslides has been lost due to 10 years of erosion, vegetation growth, human activity, and landslide boundaries becoming less distinct. For the Bolivian inventory the power-law tail of this inventory gives a landslide magnitude $m_L = 3{\cdot}6 \pm 0{\cdot}1$ so that $N_{LT} = 4100 \pm 900$ landslides. Since the number of landslides in the inventory is 1131, we conclude that the evidence for the existence of some 3000 ± 900 smaller landslides has been lost over 10–25 years.

Historical landslide inventories include the cumulative effects of many landslide events, each with their own trigger, that have occurred over tens to thousands of years. Frequency densities for three historical inventories are given in Figure 6, two from the Umbria area of Italy taken at different resolutions, and one from the Akaishi Ranges of central Japan. Also included in Figure 6, for reference, are frequency densities for the Umbria landslide event triggered by snowmelt (Figure 5).

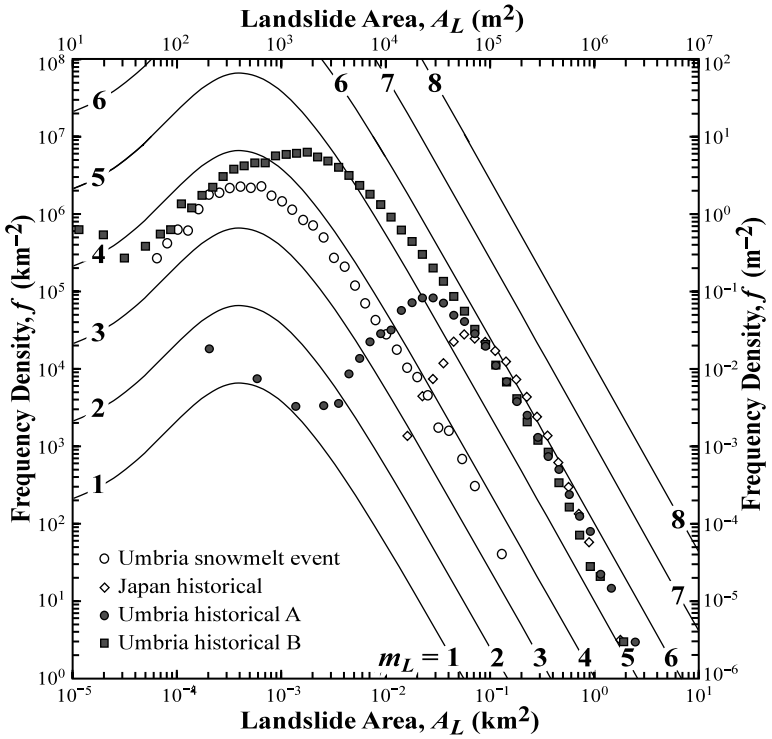

Figure 6. Dependence of the landslide frequency density f on landslide area A_L, both on logarithmic axes. Landslide frequency distributions corresponding to our proposed landslide probability distribution, Equations 3 and 35, are given for landslide magnitudes $m_L = 1, 2, \ldots, 8$ ($N_{LT} = 10, 10^2, \ldots, 10^8$). Also included are the frequency densities for four landslide inventories: the Umbria snowmelt event as in Figure 5 (open circles); 3424 historical landslides in the Akaishi Ranges of central Japan (open diamonds) (Ohmori and Sugai, 1995) estimated to have occurred in the last 10 ky; 5288 historical landslides in the Umbria region of Italy (Umbria historical A, closed circles) estimated to have occurred in the last 5–10 ky (Guzzetti *et al*., 2003a); improved resolution of the same Umbria region in Italy, 44 724 landslides (Umbria historical B, closed squares), also estimated to have occurred in the last 5–10 ky

The first example is an early reconnaissance inventory that used aerial photographs at a scale of 1:33 000 to identify $N_{LT} = 5288$ landslides in the 8456 km^2 Umbria area of Italy (Guzzetti *et al*., 2003a), estimated to have occurred in the last 5–10 thousand years (ky). This is Umbria historical data set A (filled circles, Figure 6). Subsequently a landslide inventory was obtained for this same area at a higher resolution which identified $N_{LT} = 44\,724$ landslides. This is Umbria historical data set B (filled squares, Figure 6). The two inventories are essentially identical for large landslides ($A_L > 0{\cdot}1$ km^2), but the better resolved inventory B extends agreement with the power-law tail for another order of magnitude. The power-law tail of the frequency densities are in good agreement with our landslide event probability distribution, from Equations 3 and 31, with a landslide magnitude $m_L = 5{\cdot}8 \pm 0{\cdot}1$. We hypothesize that over the last 5–10 ky the total number of landslides that have occurred in the Umbria area of Italy to be $N_{LT} = 650\,000 \pm 150\,000$. Compared with the extended inventory, $N_{LT} = 44\,724$, evidence for the existence of more than 93 per cent of the smaller original landslides has been lost.

Also included in Figure 6 is a third inventory (open circles) that includes 3424 historical landslides in the Akaishi Ranges of central Japan (Ohmori and Sugai, 1995), estimated to have occurred in the last 10 ky. The power-law tail of the frequency densities gives $m_L = 6{\cdot}0 \pm 0{\cdot}2$ so that $N_{LT} = 1\,100\,000 \pm 500\,000$. More than 99.6 ± 0.2 per cent of the smaller landslides have been lost.

LANDSLIDE EVENT MAGNITUDE VERSUS TRIGGER MAGNITUDE

Earthquakes are a major trigger for landslide events. The magnitude of an earthquake is quantified using the Richter magnitude scale. An important question is whether the magnitude of an earthquake can be related to the

magnitude of the associated landslide event. This question has been addressed by Keefer (1994). He has obtained an empirical correlation between the total volume of landslides V_{LT} triggered by an earthquake and the magnitude M of the earthquake. He considered 15 earthquakes and found

$$\log V_{LT} = 1{\cdot}45M - 11{\cdot}50 \tag{36}$$

with V_{LT} in km^3. Substituting $M = 6.7$ for the Northridge earthquake into Equation 36 gives $V_{LT} = 0{\cdot}0164$ km^3. This is less than the estimated values of $V_{LT} = 0{\cdot}099 - 0{\cdot}120$ km^3 from Table II. Although Equation 36 is clearly an approximate relation, it does provide an estimate of the total volumes of landslides generated by an earthquake. In Equation 34, we have related the landslide magnitude m_L to the total landslide volume V_{LT}. Substitution of Equation 34 into Equation 36 gives

$$m_L = 1{\cdot}29M - 5{\cdot}65 \tag{37}$$

This is an approximate relation between the earthquake magnitude M and the magnitude of the landslide event m_L triggered by the earthquake. No similar correlations are available for landslide events triggered by rainfall or snowmelt. A future goal would relate landslide-event magnitudes to quantitative measures of meteorological events.

ROCKFALL INVENTORIES

We next turn our attention to rockfall inventories, which we consider separately from other types of landslides, as we consider the applicable physics to be different. We believe that rockfalls are controlled by processes of fragmentation, compared to flows and slides that are primarily controlled by processes of slope stability.

The frequency–size distributions associated with rockfalls differ substantially from those associated with other landslide types. Rockfall inventories are usually given in terms of frequency–volume statistics rather than frequency–area statistics. Dussauge-Peisser *et al*. (2002) and Dussauge *et al*. (2003) have given cumulative frequency–volume statistics for rockfalls in (1) the Grenoble area of the French Alps, (2) Yosemite Valley, USA, and (3) worldwide. Hungr *et al*. (1999) have given cumulative frequency–volume statistics for rockfalls in southwestern British Columbia, Canada. Both sets of authors correlate their cumulative frequency–volume data with power laws, and obtain negative slopes for the medium and large rockfall events, in the range $0{\cdot}4 \pm 0{\cdot}2$. The equivalent negative slopes for the non-cumulative frequency–volume distributions are $1{\cdot}4 \pm 0{\cdot}2$. Guzzetti *et al*. (2003b) have also examined rockfalls in Yosemite Valley, USA, and fit their data to a non-cumulative frequency–volume distribution with a negative power-law exponent of about 1.1.

In Figure 7 we give the frequency density of rock falls $f = \delta N_R / \delta V_R$ as a function of rockfall volume V_R for three inventories. The first inventory includes 157 rockfalls and slides triggered by the Umbria–Marche earthquakes of September and October 1997. The second inventory consists of 135 rockfalls and slides in the Yosemite region of California during the period 1980–2002 (for details see Wieczorek *et al*., 1992, 1998; Guzzetti *et al*., 2003b). The third inventory consists of 89 historical rockfalls in the Grenoble region of France (RTM, 1997), estimated to date from the period 1904–1996 (for details see Dussauge *et al*., 2003).

Also given in Figure 7 is the power-law correlation

$$\log f(V_R) = -1{\cdot}07 \log V_R + 0{\cdot}37 \tag{38}$$

with f in km^{-3} and V_R in km^3 ($r^2 = 0{\cdot}98$). Striking differences between the densities of landslides given in Figure 5 and the densities of rockfalls given in Figure 7 include no rollover of the distribution of rockfalls for small volumes and the large numbers of small rockfalls.

Before the power-law dependence for rockfalls seen in Figure 7 can be compared with the power-law dependence for large landslides seen in Figure 5, we convert the power-law distribution of areas given in Equations 3 and 4 to a distribution of volumes.

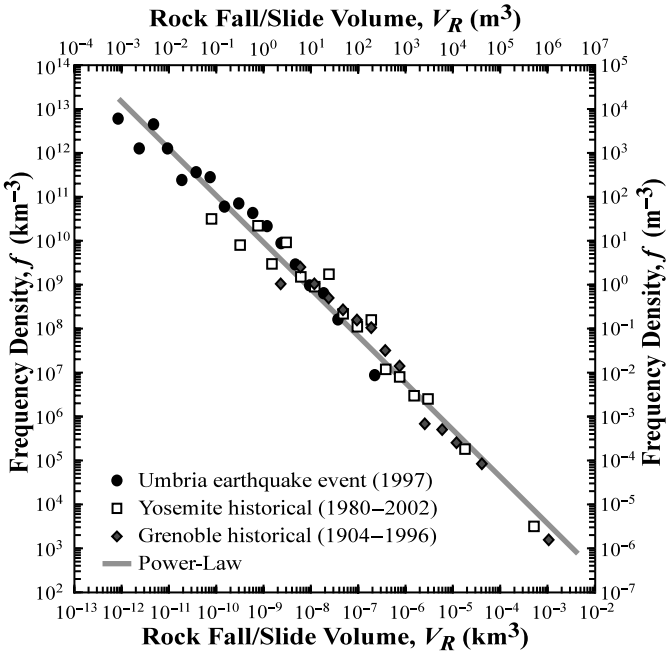

Figure 7. Dependence of the frequency density f on volume V_R for rockfall and rock-slide inventories, both on logarithmic axes. Three inventories are given: 157 rockfalls/slides triggered by the Umbria–Marche earthquakes of September and October, 1997 (closed circles); 135 rockfalls/slides in the Yosemite region, California, USA, for the period 1980–2002 (open squares) (Wieczorek *et al*., 1998); 89 historical rock falls in the Grenoble region of France, for the period 1904–1996 (closed diamonds) (RTM, 1997). The straight line is the power-law correlation given by $\log f = -1{\cdot}07 \log V_R + 0{\cdot}37$

The frequency density of landslide volumes $f(V_L)$ is related to the frequency density of landslide areas $f(A_L)$ using Equations 1 and 35 with the result

$$f(V_L) = \frac{dN_L}{dV_L} = \frac{dN_L}{dA_L}\frac{dA_L}{dV_L} = f(A_L)\frac{dA_L}{dV_L} \tag{39}$$

Accepting the power-law relation between landslide volume and area given in Equation 19, we have

$$\frac{dV_L}{dA_L} = 1{\cdot}5\varepsilon A_L^{0{\cdot}5} \tag{40}$$

Substitution of Equation 40 into Equation 39 gives

$$f(V_L) = \frac{2}{3\varepsilon A_L^{0{\cdot}5}} f(A_L) \tag{41}$$

Letting $f(A_L) = p(A_L)/N_{LT}$ and using Equation 4, this becomes

$$f(V_L) \approx \left[\frac{2a^{\rho}}{3\varepsilon N_{LT}\Gamma(\rho)}\right]\left(\frac{1}{A_L}\right)^{\rho+1{\cdot}5} \sim A_L^{-(\rho+1{\cdot}5)} \tag{42}$$

Again, using Equation 19, gives

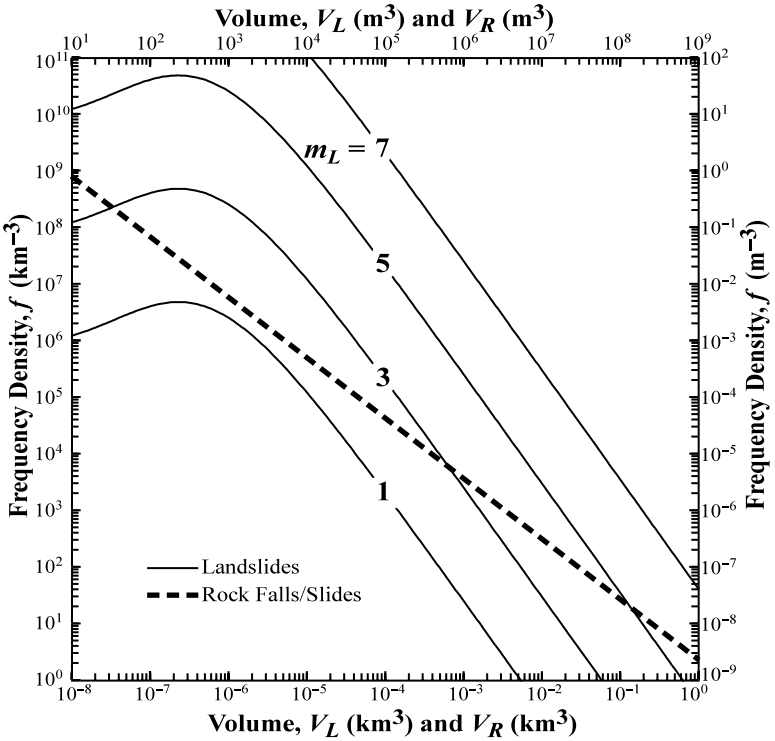

Figure 8. Dependence of the frequency density f on landslide volumes V_L and rockfall volumes V_R, using logarithmic axes. The landslide frequency distributions (thin solid lines) are given for $m_L = 1, 3, 5, 7$ ($N_{LT} = 10, 10^3, 10^5, 10^7$) and are obtained by substituting Equations 3, 19 and 35 into Equation 41. The power-law correlation (thick dashed line) for rockfalls, $\log f = -1{\cdot}07 \log V_R + 0{\cdot}37$, is from Figure 7 and Equation 38

$$f(V_L) \sim V_L^{-\left(\frac{2\rho}{3}+1\right)} \tag{43}$$

For our landslide probability distribution given in Figure 1 we have $\rho = 1{\cdot}4$ so that the tail of the corresponding probability distribution of landslide volumes is

$$f(V_L) \sim V_L^{-1{\cdot}93} \tag{44}$$

This power-law exponent of $-1{\cdot}93$ for landslide volumes differs substantially from the power-law exponent $-1{\cdot}07$ found in Figure 7 for rockfall volumes. Dussauge *et al*. (2003) also noted a substantial difference in the power-law exponent for medium and large rockfall inventories versus those inventories dominated by other types of landslides.

Landslide frequency densities are obtained as a function of landslide volume by substituting Equations 3, 19 and 35 into Equation 41. These are given in Figure 8 for $m_L = 1, 3, 5, 7$ ($N_{LT} = 10, 10^3, 10^5, 10^7$). Also included in Figure 8 is the power-law correlation for rockfalls from Equation 38. The large difference between the statistics of rockfall inventories versus landslide inventories is illustrated.

DISCUSSION

Landslide events display large variations in landslide types, sizes, distributions, patterns and triggering mechanisms. Many would question whether such complex phenomena can be quantified. We have examined three well-documented and substantially complete landslide-event inventories from different parts of the world, each with different triggering mechanisms, and find that the frequency–area statistics of all three are well approximated

by our proposed three-parameter inverse-gamma distribution (Equation 3). It is clearly desirable to test this distribution using other landslide inventories; however, the inventories must be substantially complete.

We show that our inverse-gamma landslide distribution is applicable for those substantially complete inventories dominated by flows and slides. We exclude from these inventories very long low-density debris flows – hyperconcentrated streamflows – as we believe the applicable physics more closely represents floods compared to flows and slides. Additionally, we consider rockfall-dominated inventories separately. Flows and slides are controlled primarily by slope stability processes, whereas rockfalls are controlled by the fragmentation of intact rock along joint sets.

Certainly our landslide distribution is only approximate, but is it useful? We argue that the quantification of landslides is useful in terms of estimating the role of landslides in erosional processes and in assessing landslide hazards. It is only in terms of a general landslide distribution that the landslide-event hazard can be quantified. It is based on this distribution that we have introduced a landslide-event magnitude scale to quantify landslide events. Using our distribution, we can extrapolate the largest landslide areas associated with a landslide event, to give a reasonably accurate and rapid estimate of the landslide-event magnitude, along with the total number and area of landslides in the event. This approach should be useful to hazard managers who do not have the time and resources to derive substantially complete inventories, and could provide a generally accepted measure as to the severity of a landslide event.

Based on the results given in this paper and by numerous other authors (see Introduction), medium and large landslides consistently satisfy power-law frequency–area statistics. We use for our landslide probability distribution the inverse-gamma distribution, essentially an exponential rollover for small landslides and inverse power-law decay for medium and large landslides. Other distributions have been proposed that are similar. For instance, the double Pareto probability distribution proposed by Stark and Hovius (2001) also has a power-law tail for medium and large landslides, with a rollover for smaller landslides.

One potential explanation for this power-law behaviour is the concept of self-organized criticality (Bak *et al*., 1988). This concept was introduced to explain the behaviour of the 'sandpile' model. In this model, there is a square grid of boxes. At each time step a particle is dropped into a randomly selected box. When there are four particles in a box they are redistributed to the four adjacent boxes, or in the case of boxes on the boundaries of the grid, are lost. A redistribution can lead to an 'avalanche' of redistributions; the size of the 'avalanche' is the area of boxes A_B participating in the redistributions. The non-cumulative number of 'avalanches' N_A with area A_B satisfies a power-law distribution $N_A \sim A_B^{-1{\cdot}0}$ (Kadanoff *et al*., 1989). Other models (e.g. the forest-fire model, the slider-block model) have been shown to exhibit similar behaviour (Malamud and Turcotte, 2000).

Noever (1993) and other authors have associated the power-law frequency–area statistics of large landslides with the sandpile model and the concept of self-organized criticality. However, there is a large extrapolation from the 'sandpile' model to actual landslides. In fact, for the medium and largest landslides, our best-fit power-law exponent is $-(\rho + 1) = -2{\cdot}4$, considerably larger than the model value of $-1{\cdot}0$. This is not surprising considering the simplicity of the model and the three-dimensional nature of actual landslides, and could indicate that a revision of the 'rules' for the sandpile model are needed for a realistic analogue of actual landslides in nature. Nevertheless, the relatively simple 'sandpile' model may provide the basis for understanding the power-law statistics of large landslides. In the 'sandpile' model, the region over which an avalanche will spread is well defined prior to the avalanche. Similarly, the area over which a landslide will spread can be defined before the landslide is triggered. In both, there are metastable areas. As particles are added, the metastable avalanche areas grow. As mountains grow, metastable landslide areas also grow. Detailed studies of the 'sandpile' model show that this growth is dominated by the coalescence of smaller metastable regions (Turcotte *et al*., 1999; Gabrielov *et al*., 1999; Turcotte, 1999). In addition, the coalescence cross-sections lead directly to a power-law distribution of metastable areas. It is expected that a similar coalescence and growth process would be applicable to metastable landslide areas and can explain the observed power-law frequency–area distribution of large landslides.

Other explanations for the power-law dependence have been given. Pelletier *et al*. (1997) combined a slope stability analysis with a soil-moisture analysis and obtained a power-law distribution. Hergarten and Neugebauer (1998, 2000) proposed two alternative models that give power-law distributions.

We have also shown that the non-cumulative frequency–volume distribution for rockfalls is a power law to a good approximation, although the power-law exponents for rockfall volumes (–1·1) and 'other' landslide

volumes (−1·9) are quite different. This power-law frequency–volume distribution of rockfalls may have a different cause, and is likely related to rock fragmentation.

Our hypothesis of a general frequency–area distribution for substantially complete landslide-event inventories (excluding rockfalls) clearly requires further testing. More high-quality, substantially complete inventories are required, particularly small landslide events. Our landslide distribution and the related concepts presented in this paper will potentially be of considerable value, even if only approximately valid, in helping to assess the landslide hazard and quantify the relative role of landslides to erosion.

ACKNOWLEDGEMENTS

This work has been supported by NASA Grant NAG5–9067 and is CNR–GNDCI publication number 2804. We thank C. Dussauge-Peisser, who made available to us the compilation of the Grenoble area rockfall data and T. Sugai for the landslide data from Japan. The authors would also like to thank two anonymous reviewers for their comprehensive and very helpful reviews.

REFERENCES

Abramowitz M, Segun IA. 1965. *Handbook of Mathematical Functions*. Dover: New York.

Bak P, Tang C, Wiesenfeld K. 1988. Self-organized criticality. *Physical Review* **A38**: 364–374.

Brabb EE, Harrod BL (eds). 1989. *Landslides: Extent and Economic Significance*. Balkema: Rotterdam.

Bucknam RC, Coe JA, Chavarria MM, Godt JW, Tarr AC, Bradley L-A, Rafferty S, Hancock D, Dart RL, Johnson ML. 2001. *Landslides Triggered by Hurricane Mitch in Guatemala – Inventory and Discussion*. US Geological Survey Open File Report 01–443.

Cardinali M, Guzzetti F, Brabb EE. 1990. *Preliminary map showing landslide deposits and related features in New Mexico*. US Geological Survey Open File Report 90–293.

Cardinali M, Ardizzone F, Galli M, Guzzetti F, Reichenbach P. 2000. Landslides triggered by rapid snow melting: the December 1996–January 1997 event in Central Italy. *Proceedings 1st Plinius Conference on Mediterranean Storms*. Claps P, Siccardi F (eds). Bios: Cosenza; 439–448.

Cruden DM, Varnes DJ. 1996. Landslide types and processes. In *Landslides, Investigation and Mitigation*, Turner AK, Schuster RL (eds). Special Report 247. Transportation Research Board: Washington DC; 36–75.

Dai FC, Lee CF. 2001. Frequency–volume relation and prediction of rainfall-induced landslides. *Engineering Geology* **59**: 253–266.

Dussauge C, Grasso J-R, Helmstetter A. 2003. Statistical analysis of rockfall volume distributions: Implications for rockfall dynamics. *Journal of Geophysical Research* **108(B6)**, 2286 [DOI:10.1029/2001JB000650].

Dussauge–Peisser C, Helmstetter A, Grasso J-R, Hantz D, Desvarreux P, Jeannin M, Giraud A. 2002. Probabilistic approach to rock fall hazard assessment: potential of historical data analysis. *Natural Hazards Earth System Sciences* **2**: 1–13.

Evans M, Hastings N, Peacock JB. 2000. *Statistical Distributions* (3rd edn). John Wiley: New York.

Fujii Y. 1969. Frequency distribution of landslides caused by heavy rainfall. *Journal Seismological Society Japan* **22**: 244–247.

Gabrielov A, Newman WI, Turcotte DL. 1999. An exactly soluble hierarchical clustering model: Inverse cascades, self-similarity, and scaling. *Physical Review* **E60**: 5293–5300.

Guzzetti F, Cardinali M, Reichenbach P, Carrara A. 1999. Comparing landslide maps: A case study in the upper Tiber River Basin, central Italy. *Environmental Management* **25**: 247–363.

Guzzetti F, Malamud BD, Turcotte DL, Reichenbach P. 2002. Power-law correlations of landslide areas in central Italy. *Earth and Planetary Science Letters* **195**: 169–183.

Guzzetti F, Reichenbach P, Cardinali M, Ardizzone F, Galli M. 2003a. Impact of landslides in the Umbria Region, Central Italy. *Natural Hazards and Earth System Sciences*. **3**: 469–486.

Guzzetti F, Reichenbach P, Wieczorek GF. 2003b. Rockfall hazard and risk assessment in the Yosemite Valley, California, USA. *Natural Hazards and Earth System Sciences* **3**: 491–503.

Hansen A. 1984. Landslide hazard analysis. In *Slope Instability*, Brunsden D, Prior DB (eds). John Wiley and Sons: New York; 523–602.

Harp EL, Jibson RL. 1995. *Inventory of landslides triggered by the 1994 Northridge, California earthquake*. US Geological Survey Open File Report 95–213.

Harp EL, Jibson RL. 1996. Landslides triggered by the 1994 Northridge, California earthquake. *Seismological Society of America Bulletin* **86**: S319–S332.

Hergarten S, Neugebauer HJ. 1998. Self-organized criticality in a landslide model. *Geophysical Research Letters* **25**: 801–804.

Hergarten S, Neugebauer HJ. 2000. Self-organized criticality in two-variable models. *Physical Review* **E61**: 2382–2385.

Hovius N, Stark CP, Allen PA. 1997. Sediment flux from a mountain belt derived by landslide mapping. *Geology* **25**: 231–234.

Hovius N, Stark CP, Hao-Tsu C, Jinn-Chuan L. 2000. Supply and removal of sediment in a landslide-dominated mountain belt: Central Range, Taiwan. *Journal of Geology* **108**: 73–89.

Hungr O, Evans SG, Hazzard J. 1999. Magnitude and frequency of rock falls and rock slides along the main transportation corridors of southwestern British Columbia. *Canadian Geotechnical Journal* **36**: 224–238.

Hungr O, Evans SG, Bovis MJ, Hutchnison NJ. 2001. A review of the classification of landslides of the flow type. *Environmental and Engineering Geoscience* **7**:3 221–238.

Hutchinson JN. 1988. General Report: morphological and geotechnical parameters of landslides in relation to geology and hydrogeology. In *Proceedings Fifth International Symposium on Landslides vol. 1*, Bommard C (ed.). Balkema: Rotterdam; 3–36.

IGS–WPWLI. 1990. International Geotechnical Society's UNESCO Working Party on World Landslide Inventory. A suggested method for reporting a landslide. *Bulletin International Association of Engineering Geologists* **41**: 5–12.
Johnson NL, Kotz S. 1970. *Continuous Univariate Distribution*. Houghton Mifflin: Boston.
Kadanoff LP, Nagel SR, Wu L, Zhou SM. 1989. Scaling and universality in avalanches. *Physical Review* **A39**: 6524–6533.
Keefer DK. 1984. Landslides caused by earthquakes. *Geological Society of America Bulletin* **95**: 406–421.
Keefer DK. 1994. The importance of earthquake-induced landslides to long-term slope erosion and slope-failure hazards in seismically active regions. *Geomorphology* **10**: 265–284.
Malamud BD, Turcotte DL. 2000. Cellular-automata models applied to natural hazards. *IEEE Computing in Science and Engineering* **2**: 42–51.
Noever DA. 1993. Himalayan sandpiles. *Physical Review* **E47**: 724–725.
Ohmori H, Hirano M. 1988. Magnitude, frequency and geomorphological significance of rocky mud flows, landcreep and the collapse of steep slopes. *Zeitschrift fur Geomorphology (Suppl. Bd.)* **67**: 55–65.
Ohmori H, Sugai T. 1995. Toward geomorphometric models for estimating landslide dynamics and forecasting landslide occurrence in Japanese mountains. *Zeitschrift fur Geomorphology (Suppl. Bd.)* **101**: 149–164.
Pelletier JD, Malamud BD, Blodgett T, Turcotte DL. 1997. Scale-invariance of soil moisture variability and its implications for the frequency-size distribution of landslides. *Engineering Geology* **48**: 255–268.
Pierson CP, Costa JE. 1987. A rheologic classification of subaerial sediment-water flows. In *Debris Flows/Avalanches: Process, Recognition and Mitigation*, Costa JE, Wieczorek GF (eds). Reviews in Engineering Geology VII. Geological Society of America: 1–12.
Radbruch-Hall DH, Colton RB, Davies WE, Lucchitta I, Skipp BA, Varnes DJ. 1982. *Landslide overview map of the conterminous United States*. US Geological Survey Professional Paper 1183.
Reichenbach P, Guzzetti F, Cardinali M. 1998. *Map of sites historically affected by landslides and floods*. The AVI Project, 2nd edn. CNR-GNDCI Publication Number 2116, map at 1:1 200 000 scale.
Rib HT, Liang T. 1978. Recognition and identification. In *Landslide Analysis and Control*, Schuster RL, Krizek RJ (eds). Washington Transportation Research Board Special Report 176. National Academy of Sciences: Washington DC; 34–80.
RTM. 1997. *Inventaire des mouvements rocheux, Secteur de Grenoble*. Service de Restauration des terrains en Montagne 38. Grenoble, France.
Sasaki Y, Abe M, Hirano I. 1991. Fractals of slope failure size-number distribution. *Journal Japan Society Engineering Geologists* **32**: 1–11.
Simonett DS. 1967. Landslide distribution and earthquakes in the Bewani and Torricelli Mountains, New Guinea. In *Landform Studies from Australia and New Guinea*, Jennings JN, Mabbutt JA (eds). Cambridge University Press: Cambridge; 64–84.
Speight JG. 1977. Landform pattern description from aerial photographs. *Photogrammetry* **32**: 161–182.
Stark CP, Hovius N. 2001. The characterization of landslide size distributions. *Geophysical Research Letters* **28**: 1091–1094.
Sugai T, Ohmori H, Hirano M. 1994. Rock control on magnitude-frequency distributions of landslides. *Transactions Japan Georgmorphology Union* **15**: 233–251.
Turcotte DL. 1999. Self-organized criticality. *Reports on Progress in Physics* **62**: 1377–1429.
Turcotte DL, Malamud BD, Morein G, Newman WI. 1999. An inverse-cascade model for self-organized critical behavior. *Physica* **A268**: 629–643.
Varnes DJ. 1978. Slope movements, type and processes. In *Landslide Analysis and Control*, Schuster RL, Krizek RJ (eds). Transportation Research Board, Special Report 176. National Academy of Sciences: Washington; 11–33.
Whitehouse IE, Griffiths GA. 1983. Frequency and hazard of large rock avalanches in the central Southern Alps, New Zealand. *Geology* **11**: 331–334.
Wieczorek GF. 1984. Preparing a detailed landslide-inventory map for hazard evaluation and reduction. *Bulletin Association of Engineering Geologists* **21**: 337–342.
Wieczorek GF, Snyder JB, Alger CS, Isaacson, KA. 1992. *Rock falls in Yosemite Valley, California*. US Geological Survey Open-File Report 92–387.
Wieczorek GF, Morrissey MM, Iovine G, Godt J. 1998. *Rock fall Hazards in the Yosemite Valley*. US Geological Survey Open File Report 98–467.
Yokoi Y, Carr JR, Watters RJ. 1995. Fractal character of landslides. *Environmental and Engineering Geology* **1**: 75–81.

